Hindawi
International Journal of Optics
Volume 2023, Article ID 3772408, 10 pages
https://doi.org/10.1155/2023/3772408

Research Article

The Propagation Properties of a Lorentz–Gauss Vortex Beam in a Gradient-Index Medium

Mohammed S. Qusailah, Abdu A. Alkelly, and Wafa'a A. Al-Bahry

Department of Physics, Faculty of Science, University of Sana'a, Sana'a, Yemen

Correspondence should be addressed to Abdu A. Alkelly; a.alkelly@su.edu.ye

Received 13 September 2023; Revised 10 December 2023; Accepted 13 December 2023; Published 28 December 2023

Academic Editor: Stefan Wabnitz

Based on the Huygens–Fresnel integral and ABCD matrix, the propagation equation for the Lorentz–Gauss vortex beam (LGVB) in a gradient-index medium (GRIN) is rederived. The evolution of the intensity and phase distributions of an LGVB through a GRIN medium are numerically calculated as a function of the gradient-index parameter with changes in the incident beam parameters. The results showed that the propagation path and intensity distributions changed periodically with increasing propagation distance. In contrast, phase distributions change at multiples of π/β or $2\pi/\beta$, depending on whether the M values are odd or even, respectively. At the same time, the parameters of the gradient index determine the periodic values of the Lorentz–Gauss vortex beams during propagation, and as β increased, the period of evolution decreased. The Lorentz–Gauss vortex beam propagating through the gradient index will develop from a square beam to a Gaussian vortex beam more quickly with an increase of $w_{0x} = w_{0y}$. In addition, the topological charge affects the size of the dark spot at the center of the beam and the size of the beam, causing the phase distributions to change periodically in the medium. This study is beneficial for laser optics and optical communications.

1. Introduction

Recently, with the application of single-mode diode lasers in optical sensors, fiber communication, and optical measuring instruments, a new laser beam model called the Lorentz–Gauss beam was developed to describe single-mode diode lasers [1]. The propagation properties of Lorentz–Gauss have been extensively investigated by numerous researchers. The propagation properties of Lorentz and Lorentz–Gauss beams in oceanic turbulence [2], turbulent atmospheres [3], and uniaxial crystals [4] were investigated.

A vortex beam is a particular kind of beam with a helical phase. Vortex beams' special physical characteristics make them useful for many different applications, including multidimensional optical [5], optical communications, and optical imaging [6]. The light from a single-mode diode laser is transformed into a Lorentz–Gauss vortex beam using a spiral-phase plate. The wavefront phase of a Lorentz–Gauss vortex beam can be altered using a spiral-phase plate. An advantage over a Lorentz–Gaussian beam is provided by the Lorentz–Gauss vortex beam-twisted phase front and zero intensity in the middle of the beam profile. Because a Lorentz–Gauss vortex beam contains orbital angular momentum, it may be exploited in optical micromanipulation, nonlinear optics, and quantum information processing [7]. Substantial research has been conducted on the propagation characteristics of Lorentz–Gauss vortex beams. The normalized intensity distribution, phase distribution, and orbital angular momentum density distributions were observed in the Lorentz–Gauss vortex beams traveling in free space. Investigations are made into the Lorentz–Gauss vortex beams' propagation characteristics in turbulent environments [8], substantially nonlocal nonlinear media [1], and uniaxial crystals orthogonal to the optical axis [9]. This is an edge over a Lorentz–Gaussian beam. A Lorentz–Gauss vortex beam can be used in the domains of optical micromanipulation, nonlinear optics, and quantum information processing owing to its orbital angular momentum [7]. The

propagation properties of Lorentz–Gauss vortex beams have been studied extensively. The Lorentz–Gauss vortex beams moving in free space exhibit a normalized intensity distribution, phase distribution, and orbital angular momentum density distribution [7]. The propagation properties of Lorentz–Gauss vortex beams in turbulent atmospheres [8], strongly nonlocal nonlinear media [9], and uniaxial crystals orthogonal to the optical axis [9] have been investigated.

The gradient-index (GRIN) medium has a continuous distribution and quadratic refractive index dependency. It is the most prevalent variety of nonuniform index media and may be found across the natural world. The GRIN medium offers a wide range of potential applications in focusing and image formation, optical communication, optical sensor technologies, and optical fiber construction owing to its self-focusing properties [10]. It can also be used to upgrade optical systems. As a result, they have significant optical significance in optical communication systems [11]. Recently, significant progress has been made in the research of laser beams in GRIN media. Several beams have been examined, including partially coherent modified Bessel–Gauss beams [11], vortex beams [10], and Gaussian vortex beams. The investigation of various beams, including Gaussian vortex beams [10], partially coherent modified Bessel–Gauss beams [11], vortex Hermite-cosh-Gaussian beams [12], Airy–Gaussian vortex beams [13], and on-axis and off-axis Bessel beams [14], has recently greatly advanced our understanding of laser beams in a GRIN medium. However, to the best of our knowledge, the propagation of a Lorentz–Gauss vortex beam in a gradient-index medium has not yet been reported. The propagation of a Lorentz–Gauss vortex beam in a gradient-index medium is investigated in the remainder of this study. Mathematical techniques were used to derive analytical formulae for the average intensity. We studied the effects of the gradient refractive index coefficient on the intensity, topological charge, and phase distribution.

2. Theoretical Model

In the Cartesian coordinate system, the z axis is taken to be the propagation axis. The Lorentz–Gauss vortex beam in the source plane $z = 0$ is written as follows [15]:

$$E(r_0, 0) = \frac{w_{0x} w_{0y}}{\left(w_{0x}^2 + x_0^2\right)\left(w_{0y}^2 + y_0^2\right)} \exp\left(-\frac{x_0^2 + y_0^2}{w_0^2}\right)(x_0 + i y_0)^M, \tag{1}$$

where $r_0 = (x_0, y_0)$ is the position vector at the source plane $z = 0$, w_{0x} and w_{0y} are the parameters related to the beam widths of the Lorentz part of the Lorentz–Gauss vortex in the x and y directions, respectively, w_0 is the waist width of the Gaussian part of the Lorentz–Gauss vortex beam, and M is the topological charge of the Lorentz–Gauss vortex beam. Figure 1 shows the phase and wave intensity characteristics of Lorentz–Gauss vortex beams with different $w_{0x} = w_{0y}$ for equation (1). The beam exhibits four symmetrical bright lobes. When $w_{0x} = w_{0y} = 1$ and when $w_{0x} = w_{0y}$ increases, the dark spot increases and the beam takes on a spherical shape and the direction of the phase, spiraling clockwise or anticlockwise. Figure 2 shows the phase and wave intensity characteristics of Lorentz–Gauss vortex beams with different M for equation (1). The beam exhibits four symmetrical bright lobes. When $M = 0$, the centers' total intensity is nonzero, while when $M > 0$, the center has a dark spot and phase singularity. In addition, the black spot grows, and the beam takes a quadrilateral shape as M increases. By considering, in equation (1), the relationship between the Hermite and Gauss functions and the Lorentz distribution function can be rewritten as follows [15]

$$\frac{1}{\left(w_{0x}^2 + x_0^2\right)\left(w_{0y}^2 + y_0^2\right)} = \frac{\pi}{2 w_{0x}^2 w_{0y}^2} \sum_{m=0}^{N} \sum_{n=0}^{N} \sigma_{2m} \sigma_{2n} \exp\left(-\frac{x^2}{2 w_{0x}^2} - \frac{y^2}{2 w_{0y}^2}\right) \times H_{2m}\left(\frac{x}{w_{0x}}\right) H_{2n}\left(\frac{y}{w_{0y}}\right), \tag{2}$$

where σ_{2m} and σ_{2n} are expanded coefficients that can be indexed as follows [16]:

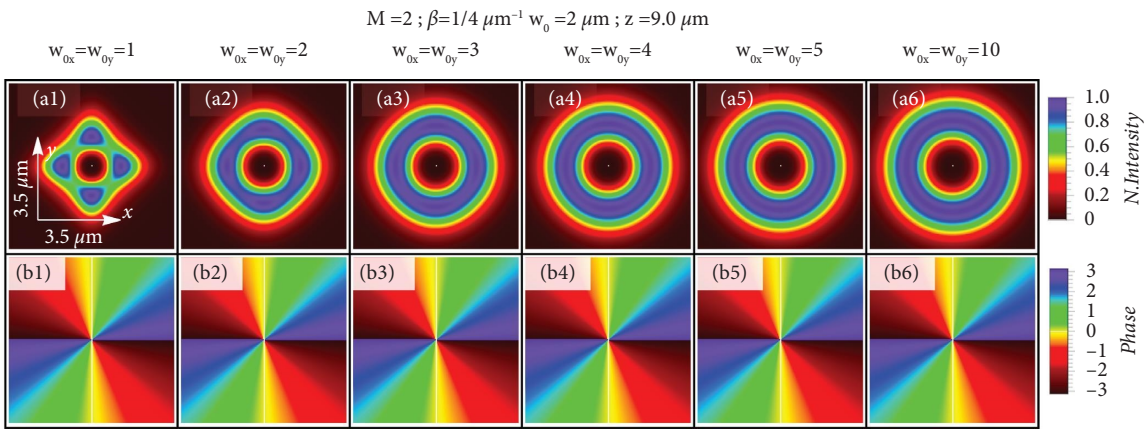

FIGURE 1: The intensity and phase distributions of the Lorentz–Gauss vortex beams at the source plane for different $w_{0x} = w_{0y}$. (a1–a6) and (b1–b6) for the intensity and phase, respectively.

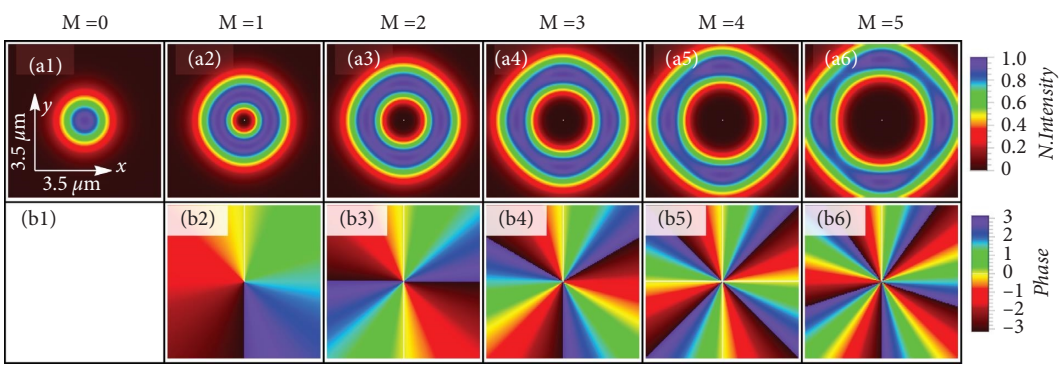

FIGURE 2: The intensity and phase distributions of the Lorentz–Gauss vortex beams at the source plane for different M. (a1–a6) and (b1–b6) for the intensity and phase, respectively.

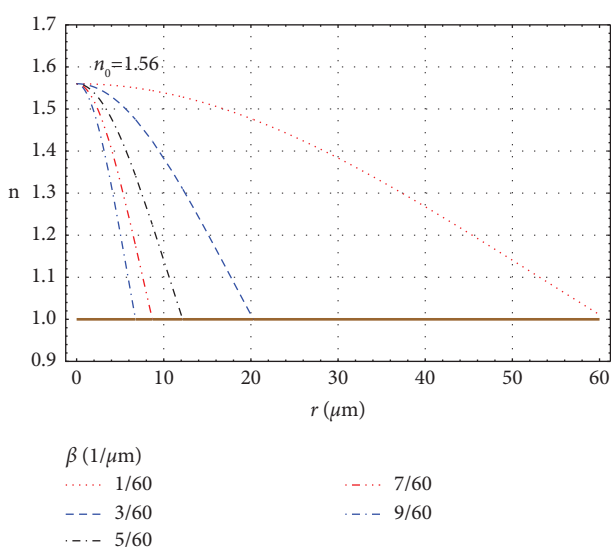

FIGURE 3: Effect of the radial component r on the radial refractive-index n for different values of $\beta = 1/60\,\{1, 3, 5, 7, 9\}\mu$m with $n_0 = 1.56$.

$$\sigma_{2n} = \frac{(-1)^n}{2^{2n-1}\sqrt{\pi}}\left\{\frac{1}{n!}\sqrt{\frac{\pi}{2}}\mathbf{e}^{1/2}\left(1-\operatorname{erf}\left(\frac{1}{\sqrt{2}}\right)\right)+\sum_{s=1}^{n}\frac{2^{2s}}{(2s)!(n-s)!}\left[\sqrt{\frac{\pi}{2}}\mathbf{e}^{1/2}\times\left(1-\operatorname{erf}\left(\frac{1}{\sqrt{2}}\right)\right)+\sum_{t=1}^{s}(-1)^t(2t-3)!!\right]\right\}. \tag{3}$$

With an increase of the even numbers $2m$ and $2n$, the values of σ_{2m} and σ_{2n} dramatically decrease. Therefore, N will not be large in numerical analysis; thus, N is set to $N = 5$. H_{2m} and H_{2n} are the $2m$- and $2n$-order Hermite polynomials, and H_{2m} can be expressed as follows [17]:

$$H_{2m}(x) = \sum_{L=0}^{m}\frac{(-1)^L(2m)!}{L!(2m-2L)!}(2x)^{2m-2L}. \tag{4}$$

Recalling the following equation [17],

$$(x+iy)^M = \sum_{L=0}^{M}\frac{M!i^L}{L!(M-L)!}x^{M-L}y^L. \tag{5}$$

Then, equation (1) can be rewritten as

$$E(r_0,0) = \frac{\pi}{2w_{0x}^2w_{0y}^2}\sum_{m=0}^{N}\sum_{n=0}^{N}\sigma_{2m}\sigma_{2n}H_{2m}\left(\frac{x}{w_{0x}}\right)H_{2n}\left(\frac{y}{w_{0y}}\right)\exp\left(-\frac{x^2}{2w_{0x}^2}-\frac{y^2}{2w_{0y}^2}\right)\times\exp\left(-\frac{x_0^2+y_0^2}{w_0^2}\right)\sum_{L=0}^{M}\frac{M!i^L}{L!(M-L)!}x_0^{M-L}y_0^L. \tag{6}$$

2.1. The Propagation Properties of an LGVB in a Gradient-Index Medium. Based on the refractive-index distribution of the gradient form, the gradient-index media were divided into three spherical, axial, and radial distributions. Radial distribution is widely applied in optical fibers. In the present paper, we are attentive to the radial gradient-index medium, with the refraction-index apportionment defined as follows [11]:

$$n(r) \simeq n_0\left(1-\frac{1}{2}\beta^2r^2\right)\text{for}\,(\beta r)^2 \ll 1, \tag{7}$$

where n_0 is the refractive index at the z axis, β is the parameter associated with the parabolic dependence of the refractive index, and $r^2 = x^2 + y^2$ is the radial component. Equation (7) represented by Figure 3.

The optical matrix connected with a GRIN medium within the paraxial approximation is expressed as follows [11]:

$$\begin{pmatrix} A & B \\ C & D \end{pmatrix} = \begin{pmatrix} \cos(\beta z) & \dfrac{\sin(\beta z)}{n_0\beta} \\ -n_0\beta\sin(\beta z) & \cos(\beta z) \end{pmatrix}. \tag{8}$$

The propagation of a Lorentz–Gauss vortex beam in a GRIN medium is governed by the Huygens–Fresnel integral diffraction that can be expressed as

$$E(r,z) = \frac{ik}{2\pi B}\int_{-\infty}^{\infty}\int_{-\infty}^{\infty}E(r_0,0)\times\exp\left\{-\frac{ik}{2B}\left[A\left(x_0^2+y_0^2\right)-2\left(x_0x+y_0y\right)+D\left(x^2+y^2\right)\right]\right\}dx_0dy_0, \tag{9}$$

where A, B, and D are the elements of the transfer matrix shown in equation (8), $k = 2\pi/\lambda$ is the wavenumber, and λ is the wavelength. By substituting equation (6) into equation (9) and recalling the following integral formula [17],

$$\int_{-\infty}^{\infty}x^n\exp\left(-px^2+2qx\right)dx = n!\exp\left(\frac{q^2}{p}\right)\left(\frac{q}{p}\right)^n\sqrt{\frac{\pi}{p}}\sum_{k=0}^{[n/2]}\frac{1}{k!(n-2k)!}\left(\frac{p}{4q^2}\right)^k = \sqrt{\frac{\pi}{p}}2^{-n}i^n\exp\left(\frac{q^2}{p}\right)\left(\frac{1}{p}\right)^{0.5n}H_n\left(-\frac{iq}{\sqrt{p}}\right), \tag{10}$$

and after doing straightforward and lengthy algebraic calculations, we can obtain

$$E(r,z)=\left(\frac{\pi}{2w_{ox}w_{0y}}\right)\left(\frac{ik}{2\pi B}\right)\exp\left(-\frac{ikD}{2B}\left(x^2+y^2\right)\right)\times\sum_{m=0}^{N}\sum_{n=0}^{N}\sigma_{2m}\sigma_{2n}\times \sum_{L=0}^{M}\frac{M!i^L}{L!(M-L)!}E(x,z)E(y,z), \tag{11}$$

where $E(x,z)$ can be expressed as

$$E(x,z)=\sqrt{\frac{\pi}{a_x}}\exp\left(-\frac{k^2x^2}{4B^2a_x}\right)\sum_{d=0}^{m}\frac{(-1)^d(2m)!}{d!(2m-2d)!} \times\left(\frac{2}{w_{0x}}\right)^{2m-2d}i^{(M-L+2m-2d)}2^{-(M-L+2m-2d)} \times\left(\frac{1}{a_x}\right)^{1/2(M-L+2m-2d)}H_{M-L+2m-2d}\left(\frac{-i}{\sqrt{a_x}}\frac{ikx}{2B}\right), \tag{12}$$

and $E(y,z)$ can be expressed as

$$E(y,z)=\sqrt{\frac{\pi}{a_y}}\exp\left(-\frac{k^2y^2}{4B^2a_y}\right)\sum_{d=0}^{n}\frac{(-1)^d(2n)!}{d!(2n-2d)!} \times\left(\frac{2}{w_{0y}}\right)^{2n-2d}i^{(L+2n-2d)}2^{-(L+2n-2d)} \times\left(\frac{1}{a_y}\right)^{1/2(L+2n-2d)}H_{L+2n-2d}\left(\frac{-i}{\sqrt{a_y}}\frac{iky}{2B}\right). \tag{13}$$

We obtain

$$a_x=\frac{1}{2w_{0x}^2}+\frac{1}{w_0^2}+\frac{ikA}{2B}, \tag{14a}$$

$$a_y=\frac{1}{2w_{0Y}^2}+\frac{1}{w_0^2}+\frac{ikA}{2B}. \tag{14b}$$

Equation (12) is the analytical expression of the Lorentz–Gauss vortex beam passing in a GRIN medium at the receiver plan z. The intensity $I(r,z)$ of the output beam is expressed as the squared modulus of the field:

$$I(r,z)=|E(r,z)|^2. \tag{15}$$

3. Simulation and Discussion

In this section, the average intensity and vortex properties of the Lorentz–Gauss vortex beam propagating in the gradient-index medium are analyzed and illustrated using equation (15). In the following numerical calculations, the parameters of the Lorentz–Gauss vortex beam in the gradient-index medium are chosen as $\lambda=0.6\mu$m, $L=\pi/\beta\mu$m, $w_0=2\mu$m, and $w_{0x}=w_{0y}=3\mu$m. In order to analyze the influences of the beam parameters on the evolution of the Lorentz–Gauss vortex beam propagating in the gradient-index medium, numerical results are given to illustrate the influences of the topological charge M, the parameters related to the beam widths of the Lorentz part of the Lorentz–Gauss vortex in the x and y directions, and the gradient-index parameter on the evolution of the transverse intensity and phase distributions with the propagation distance z.

3.1. Intensity and Phase Distributions with Different $w_{0x}=w_{0y}$. The normalized intensity distribution of the Lorentz–Gauss vortex beam with different $w_{0x}=w_{0y}$ through a gradient-index medium is shown in Figure 4(a1–a6). It can be found that when the Lorentz–Gauss vortex parameters w_{0x} and w_{0y} of the beam are equal and smaller than w_0, the beam spot is in a square shape, while when the Lorentz–-Gauss parameters w_{0x} and w_{0y} of the beam are equal and greater than w_0, the beam spot is in a circular shape. The evolutions of the phase of the Lorentz–Gauss vortex beam are shown in Figure 4(b1–b6). It is found that the phase distributions of the Lorentz–Gauss vortex beam propagating through a gradient-index medium with the difference of $w_{0x}=w_{0y}$ have the same evolution property. The phase distributions of the Lorentz–Gauss vortex beam in the gradient-index medium have the counterclockwise spiral round distribution when $w_{0x}=w_{0y}$ is larger than w_0, and the phase distributions become irregular and square spiral when $w_{0x}=w_{0y}$ is less than w_0. Figure 4(c1–c6) depicts the trajectory taken by Lorentz–Gauss vortex beams in the GRIN medium as they propagate at $w_{0x}=w_{0y}=1,2,3,5,10$.

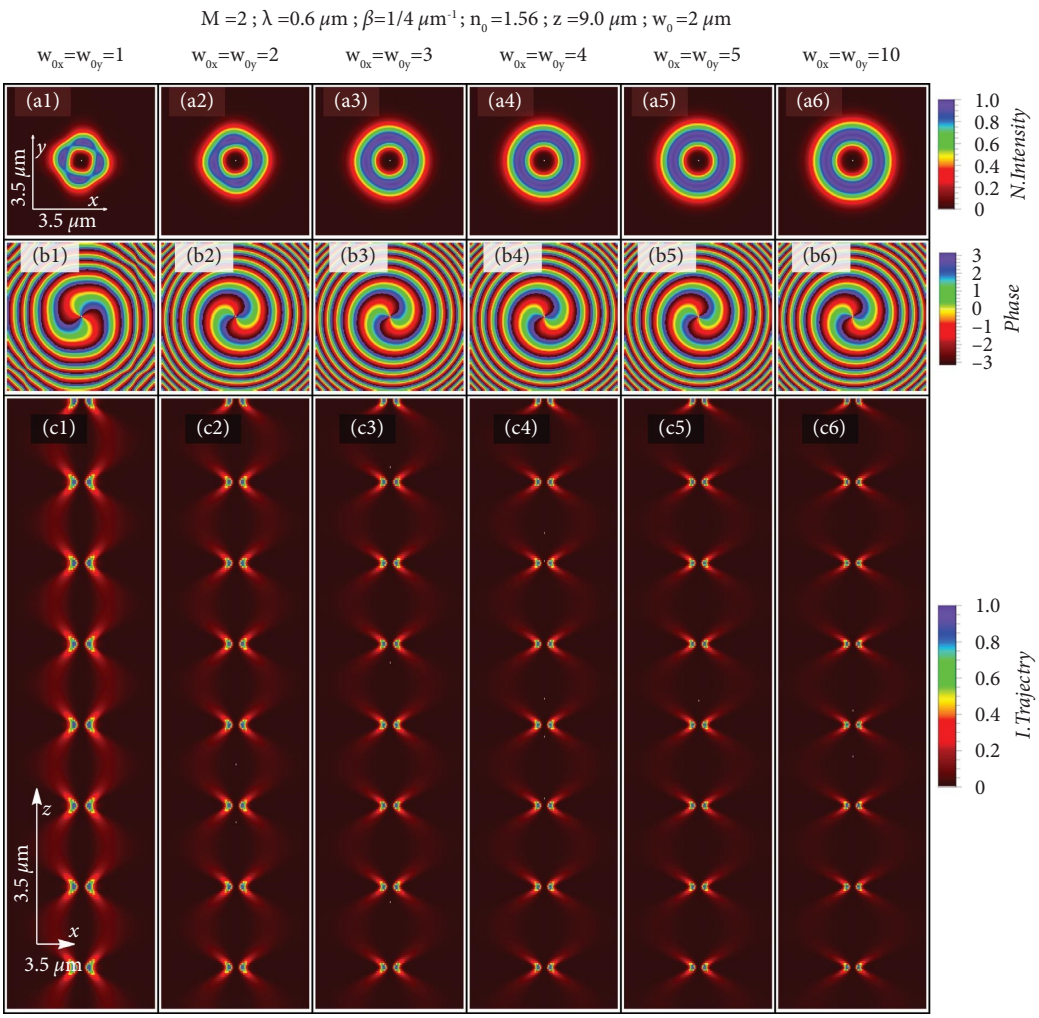

Figure 4: Numerical demonstration of the Lorentz–Gauss vortex beams propagating through the gradient-index medium with the different $w_{0x} = w_{0y}$. (a1–a6), (b1–b6), and (c1–c6) for the intensity, phase, and trajectory, respectively.

3.2. Intensity and Phase Distributions with Different Topological Charges M. The intensity and phase distributions at propagation distance $z = 9\mu$m and the propagation trajectory of the Lorentz–Gauss vortex beams with different topological charges $M = 0, 1, 2, 3, 4,$ and 5 are shown in Figure 5(a1–a6) and (b1–b6). Figure 5(a1–a6) shows that the intensity distribution is a Lorentz–Gauss beam ($z = 9\mu$m) in the case of $M = 0$. The intensity along the axis is always zero at the beam center in the focal plane during propagation when the topological charge M is large. The intensity of the beam center in the focal plane gradually diminished as M increased. In addition, when M increased, the transverse width of the beam increased. Figure 5(b1–b6) shows the normalized phase distributions with various topological charges $M = 1, 2, 3, 4,$ and 5 at $z = 9\mu$m. We found that the phase distributions of the Lorentz–Gauss vortex beam with different M have the same change in the rotation direction at the same period value of $z = 9\mu$m. Moreover, in the displayed phase for scalar Lorentz–Gauss vortex beams, some interesting petal dislocations appear in the Lorentz–Gauss distribution of the vortex beam, and the number of petals is related to the topological charge, which is equal to twice the magnitude of the topological charge of the Lorentz–Gaussian vortex beam.

3.3. Intensity and Phase Distributions along the Propagation Direction. Figure 6 shows the propagation path, intensity, and phase distributions for different propagation distances. Figures 6(a) and 5(a) shows that the Lorentz–Gauss vortex beams focus and diverge periodically during the propagation process and that the Lorentz–Gauss vortex beam propagation trajectory has a periodic distance of $L = \pi/\beta$. We notice that the intensity distributions repeat in the direction of propagation at multiples of $z = L$. Similarly, the phase repeats itself at multiples of the value $z = L$ when M values are odd but at multiples of $z = 2L$ for even values of M. As the propagation distance increased, the beam size decreased from the maximum to the lowest and then increased to a maximum, and the intensity on the axis was zero during propagation. Figures 6(a1) and (a12) show that only periodic differences in beam size allow the Lorentz–Gauss vortex intensity distributions to maintain their original circular,

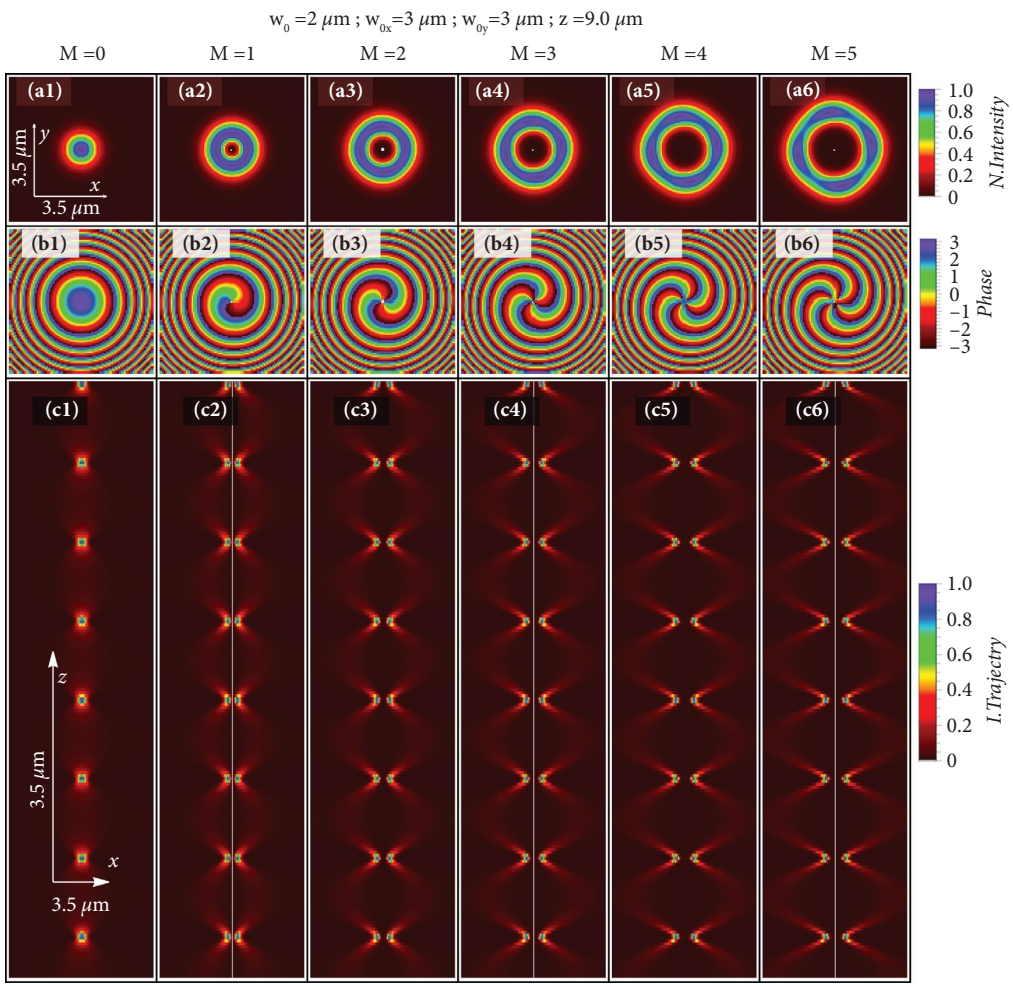

Figure 5: Numerical demonstration of the Lorentz–Gauss vortex beams propagating through the gradient-index medium with the different M. (a1–a6), (b1–b6), and (c1–c6) for the intensity, phase, and trajectory, respectively.

dark, and hollow centers while propagating along the z axis. In addition, Figures 6(b1) and (b12) display the corresponding phase distributions at specific locations taken from the phase shown in Figure 6(a). After the Lorentz–Gauss vortex beams spread across certain positions, the direction of rotation of the vortex changed from clockwise to counterclockwise. Therefore, the phased distribution takes a counterclockwise binary helical distribution in positions $z = 0.4L, 0.45L, 1.4L$, and $1.55L$ and is clockwise in positions $z = 0.55L$, $0.6L$, $1.55L$, and $1.6L$. However, the phase distribution at position $z = 1.5L$ is abnormal because the intensity on the axis is zero. In addition, the characteristics of the gradient indicator medium make the light intensity distribution differential and symmetrical in refraction, which in turn leads to a reversal of the vortex direction and a reverse change in the vortex direction owing to phase deviation effects.

3.4. Intensity and Phase Distributions with Different Gradient-Index Parameter Values of β. Figures 7(c7) and (c12) demonstrate the propagation trajectory of the Lorentz–Gauss vortex beams and the phase distributions for different values of $\beta = 1/60\{13, 14, 15, 16, 17, 18\}\,\mu$ m in the GRIN medium. Figures 7(a7) and (a12) show that Lorentz–Gauss vortex beams with different β values have the same initial beam diameter. However, the period of development of the Lorentz–Gauss vortex at the center of the gradient indicator decreased with increasing β. Therefore, β determines the periodic values of the Lorentz–Gaussian vortex beams during propagation. Figures 7(b7) and (b12) show that the phase distribution period can also be influenced by the value of β. We note that the gradient-index parameter β determines the period of self-replication of phase distributions.

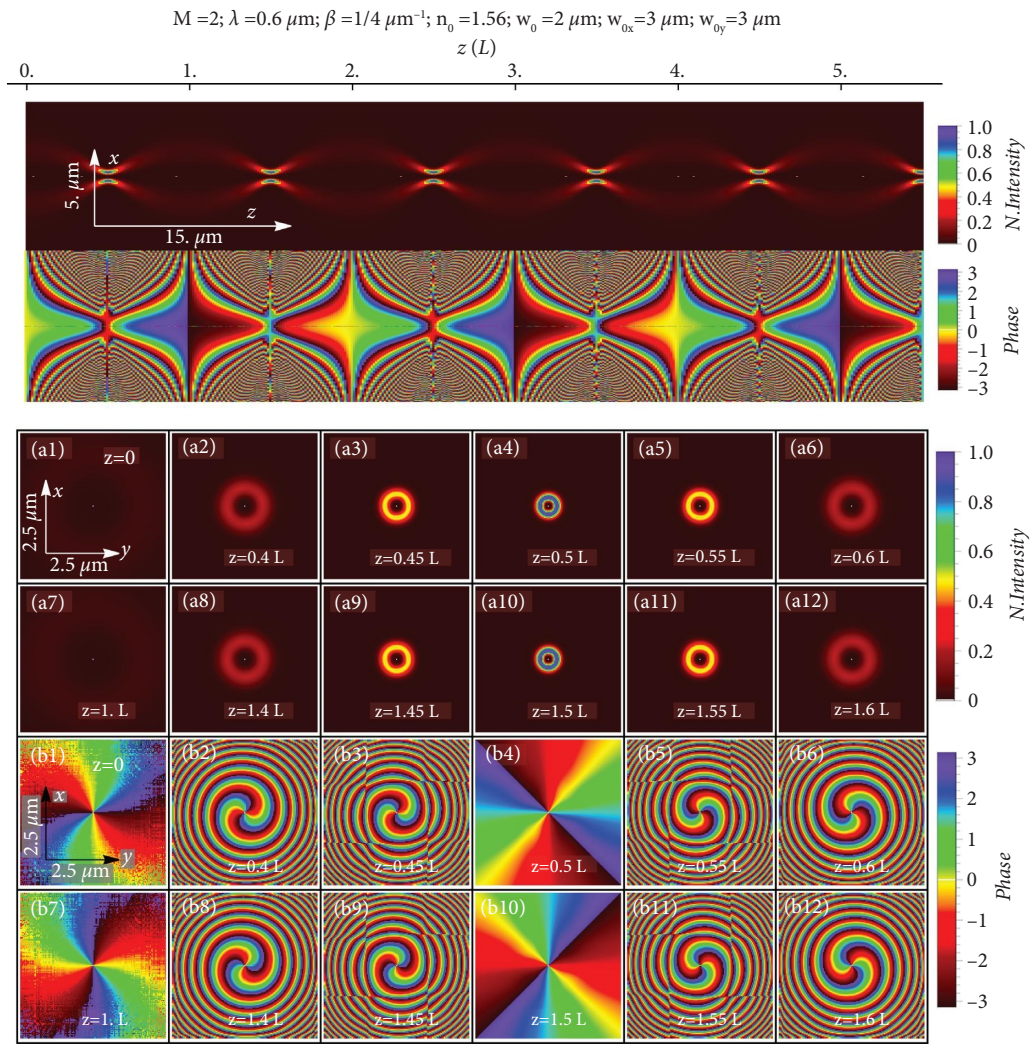

Figure 6: Numerical demonstration of the Lorentz–Gauss vortex beams propagating through the gradient-index medium. (a1–a12) and (b1–b12) for the intensity and phase, respectively.

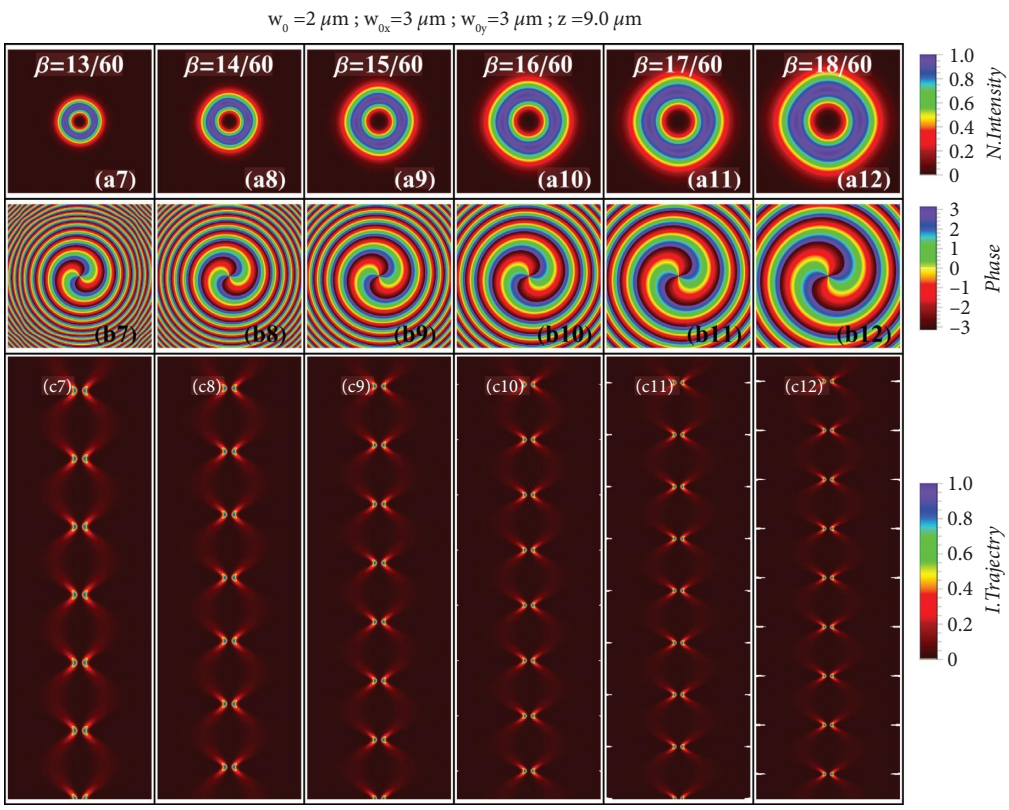

Figure 7: Numerical demonstration of the Lorentz–Gauss vortex beams propagating through the gradient-index medium. (a7–a12), (b7–b12), and (c7–c12) for the intensity, phase, and trajectory, respectively.

4. Conclusion

In this paper, based on the extended Huygens–Fresnel principle, we have derived the analytical formulae for the intensity of Lorentz–Gauss vortex beams propagating through ABCD optical systems and used them to study the change in singularities of such vortex beams within a gradient-index medium. The resulting formula allows for the numerical illustration of the evolution of the intensity and phase distributions of the beam in the GRIN medium as functions of propagation distance when the initial beam parameters and the gradient-index parameter β are changed. It is shown that the period of self-repetition of the intensity distributions and phase distributions is determined by the medium parameter β. As β increases, the evolution period decreases. The period of the phase distributions can also be impacted by the topological charge M. The Lorentz–Gauss vortex beam propagating through the gradient index will develop from a square beam to a Gaussian vortex beam more quickly with an increase $w_{0x} = w_{0y}$. The size of the circular dark hollow center and the initial spot diameter can be altered by varying M. The initial size of the spot diameter and the size of the dark, circular, and hollow center increase with increasing M. The initial size of the spot diameter and the size of the dark, circular, and hollow center increase with increasing M. In addition, it is discovered that once the Lorentz–Gauss vortex beams propagate across the sites of $z = 0.5, 1$, and $1.5L$, the rotation direction of the phase distributions is modified. In conclusion, the effect of changing the parameters of the Lorentz–Gauss vortex beam on the phase and intensity in the gradient-index medium was first studied. The present study will be helpful in understanding the shaping of Lorentz–Gauss vortex beams with a gradient-index medium, which can find applications in many areas, such as fiber communication, optical communication, and laser optics.

Data Availability

The data that support the findings of this study are available from the corresponding author upon request.

Disclosure

This study is only a master's thesis.

Conflicts of Interest

The authors declare that they have no conflicts of interest.

References

[1] G. Zhou, "Propagation property of a Lorentz–Gauss vortex beam in a strongly nonlocal nonlinear media," *Optics Communications*, vol. 330, pp. 106–112, 2014.

[2] D. Liu, Y. Wang, G. Wang, and H. Yin, "Influences of oceanic turbulence on Lorentz Gaussian beam," *Optik-International Journal for Light and Electron Optics*, vol. 154, pp. 738–747, 2018.

[3] G. Zhou and X. Chu, "Average intensity and spreading of a Lorentz-Gauss beam in turbulent atmosphere," *Optics Express*, vol. 18, p. 726, 2010.
[4] C. Zhao and Y. Cai, "Paraxial propagation of Lorentz and Lorentz-Gauss beams in uniaxial crystals orthogonal to the optical axis," *Journal of Modern Optics*, vol. 57, pp. 375–384, 2010.
[5] L. Zhu, Y. Tai, H. Li et al., "Multidimensional optical tweezers synthetized by rigid-body emulated structured light," *Photonics Research*, vol. 11, pp. 1524–1534, 2023.
[6] H. Zhang, J. Zeng, and X. Lu, "Review on fractional vortex beam," *Nanophotonics*, vol. 11, pp. 241–273, 2021.
[7] Y. Ni and G. Zhou, "Propagation of a Lorentz-Gauss vortex beam through a paraxial ABCD optical system," *Optics Communications*, vol. 291, pp. 19–25, 2013.
[8] G. Zhou and G. Ru, "Propagation of a Lorentz-Gauss vortex beam in a turbulent atmosphere," *Progress in Electromagnetics Research*, vol. 143, pp. 143–163, 2013.
[9] Y. Ni and G. Zhou, "Nonparaxial propagation of Lorentz-Gauss vortex beams in uniaxial crystals orthogonal to the optical axis," *Applied Physics B: Photophysics and Laser Chemistry*, vol. 108, no. 4, pp. 883–890, 2012.
[10] S. Yang, J. Wang, M. Guo, Z. Qin, and J. Li, "Propagation properties of Gaussian vortex beams through the gradient index medium," *Optics Communications*, vol. 465, Article ID 125559, 2020.
[11] M. Dong, Y. Bai, J. Yao, Q. Zhao, and Y. Yang, "Propagation properties of partially coherent modified Bessel–Gauss beams through the gradient-index medium," *Applied Optics*, vol. 59, p. 8023, 2020.
[12] M. Lazrek, Z. Hricha, and A. Belafhal, "Propagation of vortex Hermite-cosh-Gaussian beams in a gradient-index medium," *Optical and Quantum Electronics*, vol. 54, p. 67, 2022.
[13] R. Zhao, F. Deng, W. Yu, J. Huang, and D. Deng, "Propagation properties of Airy–Gaussian vortex beams through the gradient-index medium," *Journal of the Optical Society of America*, vol. 33, pp. 1025–1031, 2016.
[14] Z. Cao, C. Zhai, S. Xu, and Y. Chen, "Propagation of on-axis and off-axis Bessel beams in a gradient-index medium," *Journal of the Optical Society of America*, vol. 35, no. 2, pp. 230–235, 2018.
[15] D. Liu, H. Yin, G. Wang, and Y. Wang, "Propagation of partially coherent Lorentz-Gauss vortex beam through oceanic turbulence," *Applied Optics*, vol. 56, p. 8785, 2017.
[16] C. Zhao and Y. Cai, "Propagation of partially coherent Lorentz and Lorentz- Gauss beams through a paraxial ABCD optical system in a turbulent atmosphere," *Journal of Modern Optics*, vol. 58, pp. 810–818, 2011.
[17] A. Jeffrey and H. H. Dai, *Handbook of Mathematical Formulas and Integrals*, Elsevier, Amsterdam, Netherlands, 2008.